Chemical Decomposition of the TFSI Anion under Aqueous Basic Conditions

Arthur France-Lanord[1,2] Fabio Pietrucci,[3] A. Marco Saitta,[3] Jean-Marie Tarascon,[4,5]
Alexis Grimaud,[4,5] and Mathieu Salanne[1,6,5,*]

[1] *Sorbonne Université, CNRS, Physico-Chimie des Electrolytes et Nanosystèmes Interfaciaux, PHENIX, F-75005 Paris, France*

[2] *Sorbonne Université, Institut des Sciences du Calcul et des Données, ISCD, F-75005 Paris, France*

[3] *Sorbonne Université, Muséum National d'Histoire Naturelle, UMR CNRS, 7590, Institut de Minéralogie, de Physique des Matériaux et de Cosmochimie, IMPMC, F-75005 Paris, France*

[4] *Chimie du Solide et de l'Énergie, Collège de France, UMR 8260, 75231 Cedex 05 Paris, France*

[5] *Réseau sur le Stockage Electrochimique de l'Energie (RS2E), FR CNRS 3459, France*

[6] *Institut Universitaire de France (IUF), 75231 Paris Cedex 05, France*

Understanding the interfacial reactivity of aqueous electrolytes is crucial for their use in future batteries. We investigate the reactivity of the bis(trifluoromethane)sulfonimide anion when exposed to a strongly basic medium, by means of *ab initio* molecular dynamics and enhanced sampling techniques. In particular, we study the nucleophilic attack by the hydroxide anion, which was proposed as a mechanism for the formation of the solid electrolyte interphase at the negative electrode with water-in-salt electrolytes. While in the gas phase we recover a stable gaseous product, namely fluoroform, we observe the formation of trifluoromethanol in strong basic conditions, which then rapidly deprotonates to form CF_3O^-. This anion was suggested recently as a key compound leading to the formation of a solid electrolyte interphase on an Si-C anode. Such an approach could be leveraged to discover convenient additives leading to the formation of a stable interphase.

I. INTRODUCTION

In recent years, the research on aqueous batteries has been boosted by the development of water-in-salt electrolytes and their derivatives [1–3]. They enable the application of large voltages, by pushing both the anodic and the cathodic limits much further than those of conventional aqueous solutions. On the negative electrode side, this is due to the formation of a stable solid electrolyte interphase (SEI) on some materials such as Mo_6S_8, [1], but the accessible voltage window remains too far away for the conventional graphite anode. In addition, the SEI formed on the electrode was found to not be able to protect the battery against continuous electrolyte degradation during both cycling and storage [4]. Much work therefore remains to be done before the development of a practical water-in-salt electrolyte-based battery [5].

The archetypal water-in-salt is lithium bis (trifluoromethane)sulfonimide (LiTFSI) at a molality of 21 m. Under such conditions, the water molecules to Li ratio is largely below the cation coordination number under infinite dilution conditions (namely 4), so that the water molecules compete to participate to their solvation shells [1]. From the dynamics point of view, the properties of such electrolytes resemble those of ionic liquids [6]. The formation of the SEI on the anode is due to the decomposition of the anion. Although first reports interpreted it as a direct reduction of TFSI [7], it was also shown that the water molecules were involved. Indeed, the formation of H_2 showed that the hydrogen evolution reaction occurs, which leads to the formation of hydroxide anions in the vicinity of the electrode [8–10]. The OH^- can chemically react with TFSI and catalyze the formation of a fluorinated SEI [8]. However, a recent x-ray diffraction study, in which electrons are produced at the solid-liquid interface, concluded on a surface-reduction of TFSI in which no OH^- formation were observed [11]. The mechanism of SEI formation in the presence of a water-in-salt electrolyte therefore remains to be fully understood.

Knowing the decomposition process of TFSI would certainly advance the feasibility of aqueous batteries, as

degradation and growth mechanisms at the electrolyte-electrode interface control most of the properties of electrochemical devices [12–14]. One important point is whether the anion directly reacts to form CF_x-containing species and LiF, or whether reaction intermediates are involved. Indeed, it could allow us to design additives in order to control the growth and the stability of the SEI, as well as to trigger it in the case of other material chemistries. Here we show using density-functional-theory- (DFT) based molecular dynamics (MD) that the trifluoromethanolate compound can be a key reaction intermediate. We study the reactivity of TFSI in a strongly basic aqueous solution, previously investigated with experimental means [8], using enhanced sampling methods adapted to chemical reactions [15]. In this method reaction coordinates based on the coordination matrix of the atoms are used [16], which forces the reactions to occur within the limited timescale of the simulations while allowing enough flexibility to obtain unpredicted chemical products. Our results show that contrarily to the gas phase in which OH^- and TFSI react to form a well-known stable (gaseous) product, trifluoromethane (fluoroform), in the liquid phase trifluoromethanol forms and then deprotonates. This molecule is known to be highly reactive, thus providing an interesting lead to the origin of the SEI formation in the presence of water-in-salt electrolytes.

II. ATOMISTIC MODELS AND COMPUTATIONAL METHODS

Three types of system are considered: $TFSI^- + OH^-$ in vacuum (system A), and a 3 M LiOH aqueous solution containing either 100 mM of LiTFSI (system B) or a single CF_3OH molecule (system C). All initial geometries are generated using a Monte Carlo procedure, implemented in the PACKMOL [17] software. These include configurations in the reactants state as well as in the products state. For system B, the products state here corresponds to the one we expected, namely fluoroform + $N(SO_2CF_3)SO_3$. Preliminary relaxation of the models is then achieved with short classical molecular dynamics simulations, using the OPLS-AA, Joung and Cheatham, and SPC/E interatomic potentials [18–20], and the LAMMPS software [21]. Composition, box size, and total charge are reported in Table I. For subsequent DFT calculations and as required for systems with periodic boundary conditions, charged systems

are neutralized using a compensating uniformly charged background.

All DFT-based MD simulations rely on the Born-Oppenheimer approximation to the separation of ionic and electronic timescales. All simulations are performed at a temperature of 350 K. The deuterium mass for hydrogen is used to ensure satisfying energy conservation with a timestep of 0.5 fs. Systems are propagated in the canonical ensemble, using a Nosé-Hoover chain [22] of three thermostats with a time constant of 50 fs. Relaxation of systems A and B, for both reactants and products states, is achieved with unbiased DFT-based MD runs of respectively 2 and 20 ps. Computations are performed at the generalized gradient approximation (GGA) level, using the rev-PBE [23] exchange-correlation functional with D3 correction [24] for dispersion interactions. The electronic density and the wavefunction are represented using a dual basis of both plane waves and Gaussian orbitals (GPW), as implemented in the QUICKSTEP package of the CP2K program [25]. A grid cutoff of 1000 Ry with an associated relative cutoff of 60 Ry is necessary to converge the total energy, with triple-ζ plus polarization basis sets and GTH pseudopotentials (TZVP-MOLOPT-GTH). The orbital transformation method is used to self-consistently solve the Kohn-Sham equations, with a convergence criterion of 10^{-5}.

For biased simulations, we follow the approach outlined in Ref. [16] and define two collective variables, s and z, called *path* collective variables:

$$s(t) = \frac{\sum_{k=1}^{N_f} k e^{-\lambda D[\mathbf{R}(t), \mathbf{R}_k]}}{\sum_{k'=1}^{N_f} e^{-\lambda D[\mathbf{R}(t), \mathbf{R}_{k'}]}}, \quad (1)$$

$$z(t) = -\frac{1}{\lambda} \log \left(\sum_{k=1}^{N_f} e^{-\lambda D[\mathbf{R}(t), \mathbf{R}_k]} \right). \quad (2)$$

Here $N_f = 2$ is the number of reference states, λ is a free parameter, $\mathbf{R}_1$, $\mathbf{R}_2$ are the reactants and the putative products configurations, respectively, and $\mathbf{R}(t)$ is the instantaneous position vector of all the atoms of a given system. The variable s represents the progress along a reaction pathway from a given state to another one, and z the distance to this pathway. We define the similarity to reference configurations using the generalized

TABLE I. System composition, box size (side length of the cubic simulation box, in angstroms), and total charge Q. Systems A, B, and C respectively correspond to $TFSI^- + OH^-$ in vacuum, 3 M LiOH containing 100 mM of LiTFSI, and 3 M LiOH containing a single CF_3OH.

System	$N(H_2O)$	$N(TFSI^-)$	$N(Li^+)$	$N(OH^-)$	$N(CF_3OH)$	Box length (Å)	Q (e^-)
A	0	1	0	1	0	25.00	−2
B	170	1	11	10	0	17.83	0
C	170	0	10	10	1	17.80	0

distance D, i.e.,

$$D[\mathbf{R}(t), \mathbf{R}_k] = \sum_{iS} [C_{iS}(t) - C_{iS}^k]^2, \qquad (3)$$

which is the squared Euclidean distance. Here, we chose to represent a given configuration through a local description based on the coordination matrix $\mathbf{C}$. Each element C_{iS} of $\mathbf{C}$ represents the coordination of an atom i by atoms of type S. The distance is computed by summing over all matrix elements.

In a first step, the coordination is monitored during equilibration runs. The coordination of atom i by atoms of type S is computed using a common [16] switching function

$$C_{iS}(t) = \sum_{j \in S} \frac{1 - [R_{ij}(t)/R_{SS}^0]^n}{1 - [R_{ij}(t)/R_{SS}^0]^m}, \qquad (4)$$

where R_{SS}^0 is a reference distance parameter, $n = 6$ and $m = 2n$, the default values implemented in PLUMED. This specific choice allows us to capture the change of coordination of all the atoms we are tracking on the typical distances observed at the metastable states. The R_{SS}^0 values, reported in Table S1 within the Supplemental Material [26], are determined from the unbiased dynamics data, and set such that a nearest-neighbor (next-nearest-neighbor) contribution amounts to a coordination of roughly 0.9 (0.3). Converged coordination values are computed by averaging over time intervals from the unbiased dynamics data for each state (reactants and products). These values are reported in Tables S2–S5 within the Supplemental Material [26].

Finally, the λ parameter of path collective variables, which corresponds to the bandwidth of the radial basis function kernel, is set such that the distance between the reference reactants and products states times lambda is roughly equal to 2.3. For systems A and B, this corresponds to values of 0.470 and 0.309, respectively. This choice sets the reactants state at $s \sim 1.1$ and the products state at $s \sim 1.9$, allowing for easy comparison of different reactions and a smooth free-energy landscape without too-strongly localized or delocalized metastable states. Additional information on the metadynamics and umbrella sampling simulation setups are provided in the Supplementary Material [26].

III. RESULTS AND DISCUSSION

The main simulated system consists of a TFSI anion inside a basic aqueous LiOH electrolyte. Indeed, simulating directly the water-in-salt electrolyte would require too large simulation cells, and experiments have shown that the TFSI decomposes quickly under such conditions [8]. DFT-based MD is the method of choice for studying chemical reactions in the liquid phase, but it requires

biasing the system along reaction coordinates in order to overcome the free-energy barriers [27]. In the present work, two reaction coordinates are built by determining the coordination matrix of a selection of atoms in the reactants and products states. The former is easily chosen since the initial compounds are known. Concerning the products, since the computational cost of DFT-based MD prevents us from exploring a plethora of scenarios, we choose to follow the hypothesis made in Ref. [8]: based on the larger Mulliken charge carried by the sulfur atom within TFSI [28,29], a nucleophilic attack of OH$^-$ on this site was suggested. Weakening of the C—S bond by OH$^-$ in an Mg(TFSI)$_2$-diglyme electrolyte was also investigated previously [30]. Finally, C—S bond cleavage was also observed from reductive decomposition of TFSI studied using an *ab initio*-classical hybrid scheme [31]. We therefore choose trifluoromethane and the N(SO$_2$CF$_3$)SO$_3$ anion as the probable products of this first step, as illustrated in Fig. 1 (which also gives the coordination matrices for the two states). The first reaction coordinate (s) follows the advancement of the reaction, while the second one (z) allows the system to deviate from the direct pathway between the reactants and products states. We then use metadynamics [32], an enhanced sampling method that allows us to progressively escape from free-energy minima. The main interest of this simulation setup is enforcing the system to react without having necessarily to reach the guessed products state: any other products can be formed. Once a reactive pathway is obtained, the free-energy profile is computed using umbrella sampling.

In order to validate the method, the reaction is first enforced on isolated compounds, i.e., in the absence of any solvent or other species. The free-energy profile obtained is shown in Fig. 2(a). It is clear that the method allows us to easily and efficiently pass from one state to the other. However, the free energy is large for the reactants state due to a significant contribution of the unscreened anion-anion repulsion. The products have the lowest free energy, confirming that they are a good guess for the final state. The reaction occurs through the approach of the O atom from the hydroxide to one of the S atoms from the TFSI, which leads to the breaking of the corresponding C—S bond (see Supplemental Video 1 [26]). The carbon atom attracts the hydrogen from the hydroxide, resulting in the formation of a fluoroform molecule.

In the basic solution, the results are very different. The metadynamics does not bring the system towards the same products, as shown on Fig. 2(b). Instead, it forms trifluoromethanol (CF$_3$OH) and N(SO$_2$CF$_3$)(SO$_2$)$^{2-}$. The latter anion has been previously identified as a product of the radiolytic decomposition of ionic liquids involving TFSI [33,34]. We can only speculate that in an environment involving strong Lewis acids such as Li$^+$ cations, further decomposition will occur. Contrarily to the gas phase, the reactants display a lower free energy because
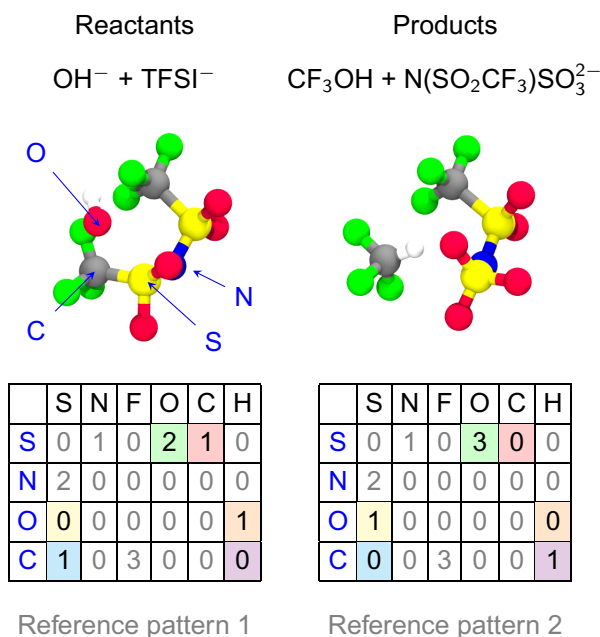
FIG. 1. Initial hypothesis of reactants and products, along with coordination matrices used in path collective variables. Special atoms corresponding to row entries of the coordination matrices are labeled in blue in the reactants state. Matrix elements whose values change when going from reactants to products are highlighted using colors in the coordination matrices.

FIG. 2. Free-energy landscapes obtained from umbrella sampling, in the (s, z) space. (a) Reaction in vacuum, (b) reaction in the basic solution. An example of the geometry is shown for each metastable state, at $s \sim 1.1$, $s \sim 1.9$, and $s \sim 1.5$. The cross corresponds to the location of the transition state identified further on.

the Coulombic interactions are screened by the presence of the electrolyte. The products are largely metastable, displaying a free energy of 206 kJ mol^{-1}: such an unfavorable state certainly indicates intermediates, which should further decompose rapidly. Based on the converged free-energy profile, the putative transition state (TS) has a free energy of 298 kJ mol^{-1}. The largest statistical error on the free energy is of about 11 kJ mol^{-1}, as explained in the Supplemental Material [26]. In order to determine precisely the position of the TS, we perform a committor analysis. This approach consists of picking several configurations along the transition pathway and performing a series of short (1 ps) simulations by randomly drawing initial velocities from the Maxwell-Boltzmann distribution. If the point is located before (respectively after) the TS, the trajectories will mostly evolve towards the reactants (respectively products) state, while close to the TS, they will share evenly between the two. The results for three points, as well as the structure of the deduced TS, are shown on Fig. 3. Contrarily to the gas phase, the OH$^-$ reacts with the TFSI with a nucleophilic substitution mechanism. In the TS the three C—F bonds lie within the same plane, with the oxygen and the sulfur atoms lying on the two sides of the plane (with corresponding C-O and C-S distances of 2.49 and 3.21 Å). Supplemental Video 2 [26] shows the reactive event.

It is then interesting to understand why this second reaction pathway is favored in the basic solution. A first
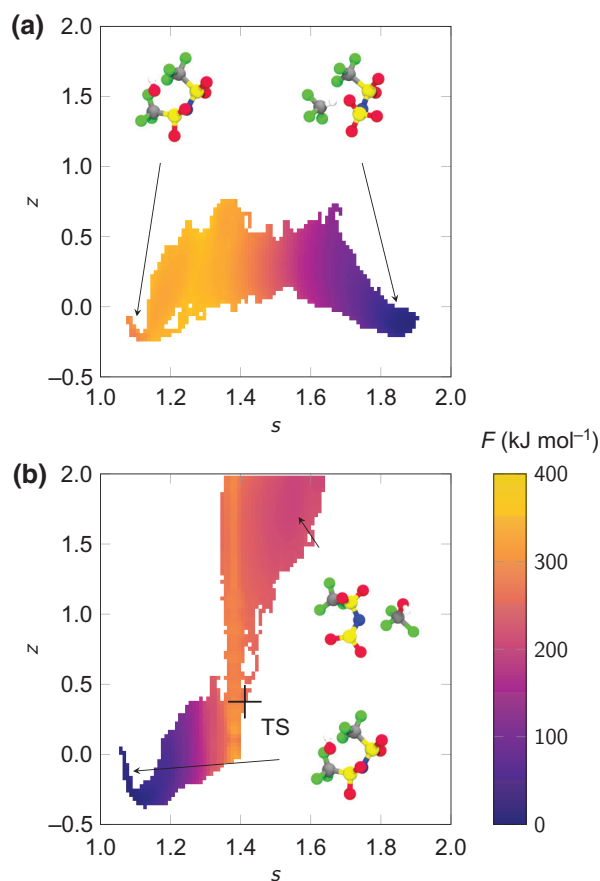
hint would be that the OH$^-$ anions do not sufficiently approach the S—C bond. In order to check this point, we compute the radial distribution function $g(r)$ between the sulfur from TFSI, and the oxygen from either OH$^-$ or H$_2$O molecules. These results are reported in Figs. 4(a) and 4(b). As can be seen from the first peak located at 4 Å, both the hydroxide ions and water molecules are found in the surroundings of the TFSI's S—C bonds, although never as close as in the case of the gas phase TS (the corresponding distances are shown as gray lines in the two plots). This is also shown in Figure S5 within the Supplemental Material [26], which displays the shortest distances over the course of the trajectories. It is then necessary to understand why the hydroxide ions do not react with the TFSI. We thus attempt to force the formation of the expected trifluoromethane and N(SO$_2$CF$_3$)SO$_3$ products in the basic solution, by transferring the TS geometry obtained from the gas phase calculation to a liquid system. More details concerning the procedure are included in Section 6 of the Supplemental Material [26].
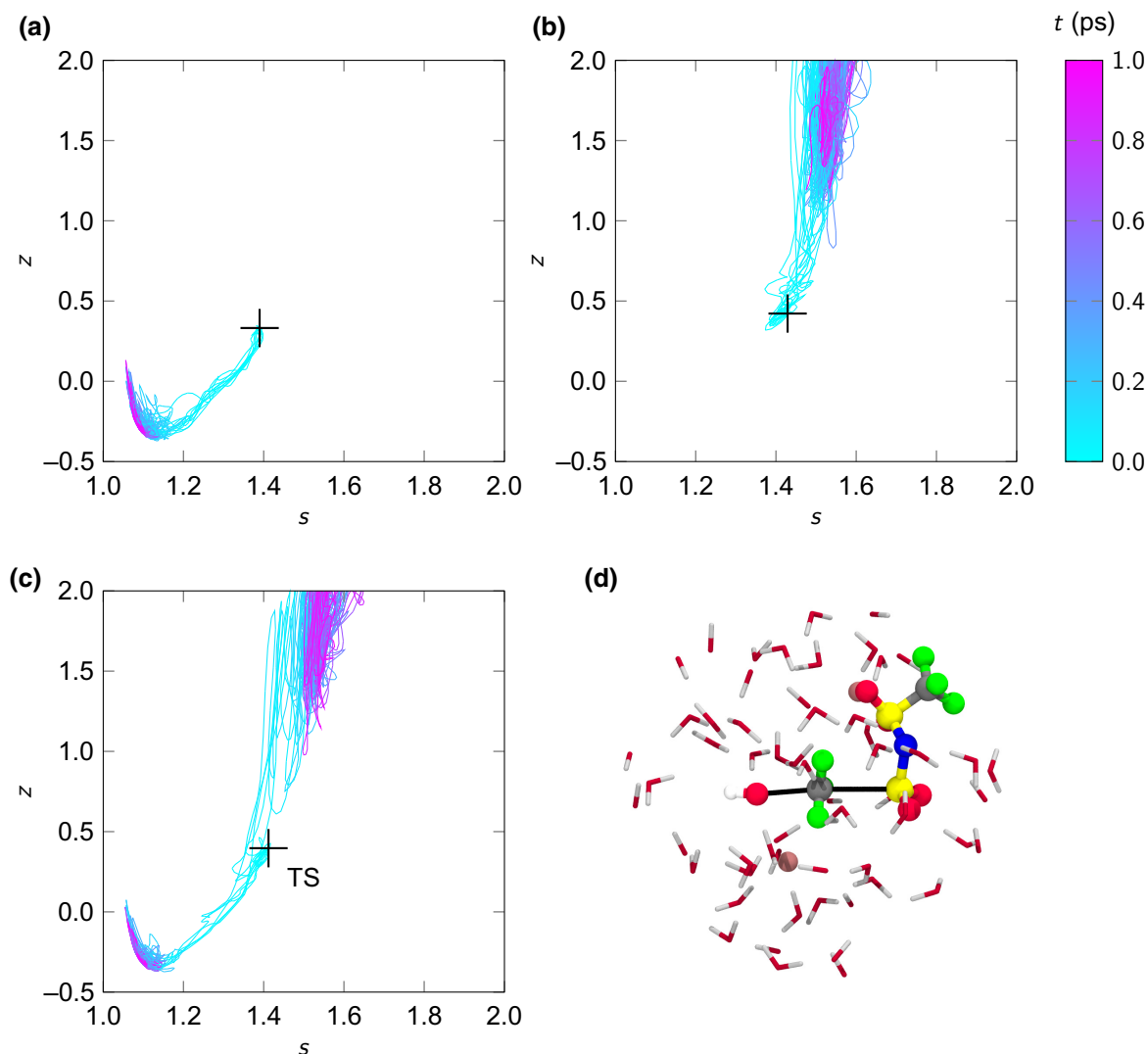
FIG. 3. Ten independent trajectories starting from the same position in (s, z) space [(a) $s = 1.39$, $z = 0.33$, (b) $s = 1.43$, $z = 0.42$, (c) $s = 1.41$, $z = 0.40$], with randomized initial velocities. The color corresponds to the simulation time, going from cyan to magenta. The crosses denote the initial configuration positions in the (s, z) space. The starting point in panel (c) corresponds to a member of the transition state ensemble. (d) Geometry of the identified transition state of panel (c). Black lines emphasize the O-C and C-S distances of 2.49 and 3.21 Å, respectively.

We simulate 100 committor trajectories from the gas phase TS in solution, with randomized velocities. In each case, the system relaxes to the reactants state, showing that this geometry is no longer a good TS once immersed in the basic solution. This can be due to either energetic or entropic constraints on how reactant molecules must arrange to form the expected products. In Figs. 4(c) and 4(d), we show the time-dependent distances between the sulfur (carbon) from TFSI and the oxygen (hydrogen) from OH⁻, over the course of the 100 committor trajectories mentioned above. Both distances overall increase over time. At short times ($t < 25$ fs), the hydrogen moves away from the TFSI faster than the oxygen, owing to its lighter mass, as well as to its propensity to form hydrogen bonds

with water molecules [35]. As can be seen in Fig. 4(e), upon relaxing to the reactants state, the anion readily forms hydrogen bonds with the surrounding water network. Consequently, the hydroxide orientation becomes unfavorable for a nucleophilic attack to occur. On the contrary, to form the trifluoromethanol product, an OH⁻ only needs to line up with the S—C bond, as can be seen in Supplementary Video 2 [26]—its hydrogen atom still keeps the freedom to form hydrogen bonds with the nearby water molecules.

We now discuss the reactivity of CF_3OH. Unlike the trifluoromethane that was initially envisaged, it does not form stable gaseous molecules. In the gas phase, trifluoromethanol eliminates HF in well-studied unimolecular reaction processes [36–39]. It is however highly
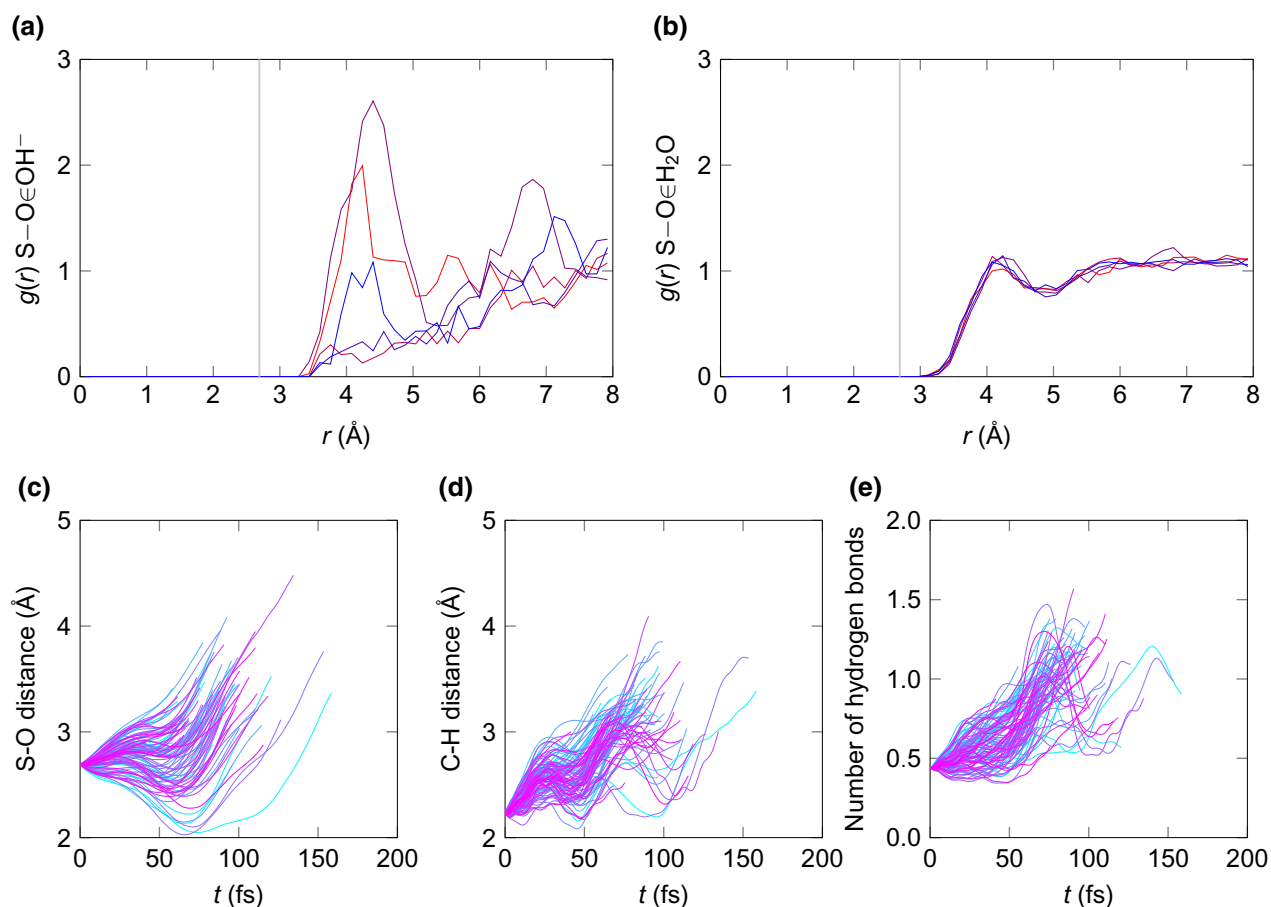
FIG. 4.   Top: radial distribution functions computed over 20-ps-long unbiased equilibrium trajectories of the reactants in the basic solution, between the sulfur from TFSI and the oxygen from either hydroxide anions (a) or water molecules (b). Each color corresponds to an independent trajectory. Gray lines correspond to the distances in the gas phase transition state geometry. Bottom: observables computed from the 100 committor trajectories starting from the solvated gas phase geometry. (c) Distance between the sulfur from TFSI and the oxygen from OH^-, (d) distance between the carbon from TFSI and the hydrogen from OH^-, (e) number of hydrogen bonds involving OH^-. Each color corresponds to an independent trajectory.

unlikely to observe such a reaction in an aqueous basic environment, in which trifluoromethanol should act as a proton donor. By performing further equilibrium simulations of CF_3OH, still in the basic solution, we observe a quick deprotonation to form the CF_3O^- anion, as shown in Fig. 5. CF_3O^- reactivity towards a series of molecules was studied in the framework of atmospheric chemistry [40]. In the gas phase, it was shown to react rapidly with many compounds ($ClONO_2$, HO_2NO_2, SO_2, etc.) by transferring fluoride, and it hydrolyzes in aqueous solution to form F^-, HF, and CO_2. However, in the case of the water-in-salt-electrolyte and/or of the basic aqueous solution studied here, its reactivity may differ due to the presence of Li^+, which is a strong Lewis acid (and is present under large concentrations). In a recent study on the use of dioxolone derivatives for high-energy-density lithium-ion batteries, the reaction

$$CF_3O^- + Li^+ \longrightarrow CF_2O + LiF \tag{5}$$
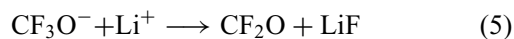
was suggested as a key step for the formation of the SEI on a Si-C anode [41]. It is therefore possible that this compound also plays a role in the formation of the SEI in water-in-salt-based aqueous ion batteries.

In conclusion, we have shown that the TFSI anion reacts differently with the hydroxide anion in the gas phase and in aqueous basic solutions. In the gas phase, the reaction occurs through an attack of the C—S bond to form fluoroform, while in the liquid phase the hydrogen bond network hinders the hydroxide to orientate in order to form the new C—H bond. Instead, the reaction occurs via a nucleophilic attack on the carbon atom, leading to the formation of trifluoromethanol, which quickly loses its proton to form CF_3O^-. This species is a well-known fluorinating agent, so that its formation as a reaction intermediate provides an explanation of the composition of the SEI in water-in-salt-based aqueous batteries. In future years, designing the SEI using well-targeted additives will be a key towards more efficient batteries with longer cycle life. Although
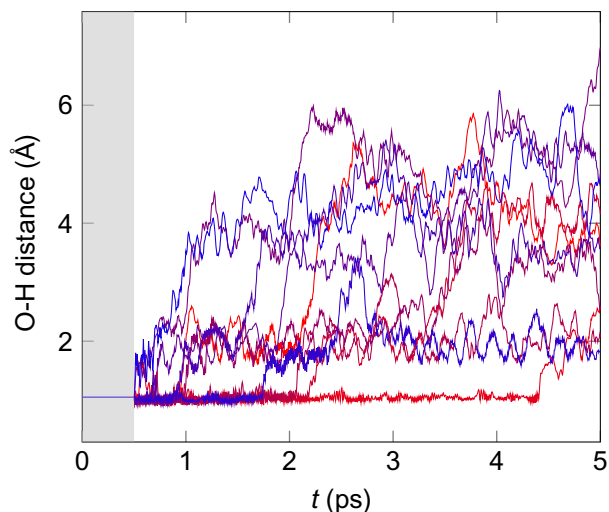
FIG. 5. The O-H distance in trifluoromethanol plotted as a function of simulation time for ten independent trajectories. The gray box corresponds to the first 0.5 ps, in which the molecule's geometry is frozen. In all trajectories, the proton quickly leaves the molecule in order to form CF_3O^-.

trifluoromethanol is not a convenient solution in this respect because its synthesis requires complex conditions [42], finding other compounds that could generate it *in situ* during the first cycles of the battery would be an interesting lead for future research. This work also emphasizes the importance of taking into account the environment when modeling chemical reactions occurring in batteries, as was previously shown for prebiotic chemistry [16]. Indeed, in the case of SEI growth, if the reaction pathways and products depend on the medium in which chemical species evolve, the environment will eventually dictate the features of the SEI, including its structure and stability.

ACKNOWLEDGMENTS

[1] L. Suo, O. Borodin, T. Gao, M. Olguin, J. Ho, X. Fan, C. Luo, C. Wang, and K. Xu, "Water-in-salt" electrolyte enables high-voltage aqueous lithium-ion chemistries, Science **350,** 938 (2015).

[2] C. Yang, J. Chen, T. Qing, X. Fan, W. Sun, A. von Cresce, M. S. Ding, O. Borodin, J. Vatamanu, M. A. Schroeder, N. Eidson, C. Wang, and K. Xu, 4.0 V Aqueous Li-ion batteries, Joule **1,** 122 (2017).

[3] M. Amiri and D. Bélanger, Physicochemical and electrochemical properties of water-in-salt electrolytes, ChemSus Chem **14,** 2487 (2021).

[4] L. Droguet, A. Grimaud, O. Fontaine, and J.-M. Tarascon, Water-in-salt electrolyte (WiSE) for aqueous batteries: A long way to practicality, Adv. Ener. Mater. **10,** 2002440 (2020).

[5] P. Jaumaux, X. Yang, B. Zhang, J. Safaei, X. Tang, D. Zhou, C. Wang, and G. Wang, Localized water-in-salt electrolyte for aqueous lithium-ion batteries, Angew. Chem. Int. Ed. **60,** 19965 (2021).

[6] Z. Li, R. Bouchal, T. Mendez-Morales, A.-L. Rollet, C. Rizzi, S. Le Vot, F. Favier, B. Rotenberg, O. Borodin, O. Fontaine, and M. Salanne, Transport properties of Li-TFSI water-in-salt electrolytes, J. Phys. Chem. B **123,** 10514 (2019).

[7] L. Suo, D. Oh, Y. Lin, Z. Zhuo, O. Borodin, T. Gao, F. Wang, A. Kushima, Z. Wang, H.-C. Kim, Y. Qi, W. Yang, F. Pan, J. Li, K. Xu, and C. Wang, How solid-electrolyte interphase forms in aqueous electrolytes, J. Am. Chem. Soc. **139,** 18670 (2017).

[8] N. Dubouis, P. Lemaire, B. Mirvaux, E. Salager, M. Deschamps, and A. Grimaud, The role of the hydrogen evolution reaction in the solid-electrolyte interphase formation mechanism for "Water-in-Salt" electrolytes, Energy Environ. Sci. **11,** 3491 (2018).

[9] R. Bouchal, Z. Li, C. Bongu, S. Le Vot, R. Berthelot, B. Rotenberg, F. Favier, S. Freunberger, M. Salanne, and O. Fontaine, Competitive salt precipitation/dissolution during free-water reduction in water-in-salt electrolyte, Angew. Chem. Int. Ed. **59,** 15913 (2020).

[10] Y. Kim, M. Hong, H. Oh, Y. Kim, H. Suyama, S. Nakanishi, and H. R. Byon, Solid electrolyte interphase revealing interfacial electrochemistry on highly oriented pyrolytic graphite in a water-in-salt electrolyte, J. Phys. Chem. C **124,** 20135 (2020).

[11] H.-G. Steinrück, C. Cao, M. Lukatskaya, C. Takacs, G. Wan, D. Mackanic, Y. Tsao, J. Zhao, B. Helms, K. Xu, O. Borodin, J. F. Wishart, and M. Toney, Interfacial dspeciation determines interfacial chemistry: X-ray-induced lithium fluoride formation from water-in-salt electrolytes on solid surfaces, Angew. Chem. Int. Ed. **59,** 23180 (2020).

[12] B. Wang, S. M. Alhassan, and S. T. Pantelides, Formation of Large Polysulfide Complexes during the Lithium-Sulfur Battery Discharge, Phys. Rev. Appl. **2,** 034004 (2014).

[13] M. Liu, M. Seita, T. Duong, W. C. H. Kuo, and M. J. Demkowicz, Preferential corrosion of coherent twin boundaries in pure nickel under cathodic charging, Phys. Rev. Mater. **3,** 063606 (2019).

[14] S. Begić, F. Chen, E. Jónsson, and M. Forsyth, Water as a catalyst for ion transport across the electrical double layer in ionic liquids, Phys. Rev. Mater. **4,** 045801 (2020).

[15] A. M. Saitta and F. Saija, Miller experiments in atomistic computer simulations, Proc. Natl. Acad. Sci. U.S.A. **111,** 13768 (2014).

[16] F. Pietrucci and A. M. Saitta, Formamide reaction network in gas phase and solution via a unified theoretical approach:

Toward a reconciliation of different prebiotic scenarios, Proc. Natl. Acad. Sci. U.S.A. **112**, 15030 (2015).

[17] L. Martínez, R. Andrade, E. G. Birgin, and J. M. Martínez, PACKMOL: A package for building initial configurations for molecular dynamics simulations, J. Comput. Chem. **30**, 2157 (2009).

[18] J. N. Canongia Lopes and A. A. Pádua, Molecular force field for ionic liquids composed of triflate or bistriflylimide anions, J. Phys. Chem. B **108**, 16893 (2004).

[19] I. S. Joung and T. E. Cheatham III, Determination of alkali and halide monovalent ion parameters for use in explicitly solvated biomolecular simulations, J. Phys. Chem. B **112**, 9020 (2008).

[20] H. J. C. Berendsen, J. R. Grigera, and T. P. Straatsma, The missing term in effective pair potentials, J Phys. Chem. **91**, 6269 (1987).

[21] A. P. Thompson, H. M. Aktulga, R. Berger, D. S. Bolintineanu, W. M. Brown, P. S. Crozier, P. J. in 't Veld, A. Kohlmeyer, S. G. Moore, T. D. Nguyen, R. Shan, M. J. Stevens, J. Tranchida, C. Trott, and S. J. Plimpton, LAMMPS - a flexible simulation tool for particle-based materials modeling at the atomic, meso, and continuum scales, Comput. Phys. Commun. **271**, 108171 (2022).

[22] G. J. Martyna, M. L. Klein, and M. E. Tuckerman, Nosé–Hoover chains: the canonical ensemble via continuous dynamics, J. Chem. Phys. **97**, 2635 (1992).

[23] Y. Zhang and W. Yang, Comment on "Generalized Gradient Approximation Made Simple", Phys. Rev. Lett. **80**, 890 (1998).

[24] S. Grimme, J. Antony, S. Ehrlich, and H. Krieg, A consistent and accurate ab initio parametrization of density functional dispersion correction (DFT-D) for the 94 elements H-Pu, J. Chem. Phys. **132**, 154104 (2010).

[25] T. D. Kühne *et al.*, CP2K: An electronic structure and molecular dynamics software package - Quickstep: Efficient and accurate electronic structure calculations, J. Chem. Phys. **152**, 194103 (2020).

[26] See Supplemental Material at http://link.aps.org/supplemental/10.1103/PRXEnergy.1.013005, which includes Refs. [16,32,43–46], for (a) the coordination matrices for path collective variables; (b) additional details on the metadynamics, commitor analysis, and umbrella sampling simulations; (c) additional data on the trifluoromethanol deprotonation and gas phase transition state geometry in solution; and (d) details on the hydrogen bond determination.

[27] D. Branduardi, F. L. Gervasio, and M. Parrinello, From A to B in free energy space, J. Chem. Phys. **126**, 054103 (2007).

[28] D. Benrabah, R. Arnaud, and J.-Y. Sanchez, Comparative ab initio calculations on several salts, Electrochim. Acta **40**, 2437 (1995).

[29] I. Rey, P. Johansson, J. Lindgren, J. C. Lassègues, J. Grondin, and L. Servant, Spectroscopic and Theoretical Study of $(CF_3SO_2)_2N^-$ (TFSI$^-$) and $(CF_3SO_2)_2NH$ (HTFSI), J. Phys. Chem. A **102**, 3249 (1998).

[30] Y. Yu, A. Baskin, C. Valero-Vidal, N. T. Hahn, Q. Liu, K. R. Zavadil, B. W. Eichhorn, D. Prendergast, and E. J. Crumlin, Instability at the electrode/electrolyte interface induced by hard cation chelation and nucleophilic attack, Chem. Mater. **29**, 8504 (2017).

[31] Y. Liu, P. Yu, Y. Wu, H. Yang, M. Xie, L. Huai, W. A. Goddard III, and T. Cheng, The DFT-ReaxFF hybrid reactive dynamics method with application to the reductive decomposition reaction of the TFSI and DOL electrolyte at a lithium–metal anode surface, J. Phys. Chem. Lett. **12**, 1300 (2021).

[32] A. Laio and M. Parrinello, Escaping free-energy minima, Proc. Natl. Acad. Sci. U.S.A. **99**, 12562 (2002).

[33] É. Bossé, L. Berthon, N. Zorz, J. Monget, C. Berthon, I. Bisel, S. Legand, and P. Moisy, Stability of [MeBu$_3$N][Tf$_2$N] under gamma irradiation, Dalton Trans. **37**, 924 (2008).

[34] L. Yuan, C. Xu, J. Peng, L. Xu, M. Zhai, J. Li, G. Wei, and X. Shen, Identification of the radiolytic product of hydrophobic ionic liquid [C$_4$mim][NTf$_2$] during removal of Sr^{2+} from aqueous solution, Dalton Trans. **38**, 7873 (2009).

[35] D. Marx, A. Chandra, and M. E. Tuckerman, Aqueous basic solutions: Hydroxide solvation, structural diffusion, and comparison to the hydrated proton, Chem. Rev. **110**, 2174 (2010).

[36] J. Francisco, An examination of primary and secondary dissociation pathways of trifluoromethanol: identification of plausible routes leading to the formation of hydrogen fluoride, Chem. Phys. **150**, 19 (1991).

[37] K. Brudnik, D. Wójcik-Pastuszka, J. T. Jodkowski, and J. Leszczynski, Theoretical study of the kinetics and mechanism of the decomposition of trifluoromethanol, trichloromethanol, and tribromomethanol in the gas phase, J. Mol. Model. **14**, 1159 (2008).

[38] M. T. Nguyen, M. H. Matus, V. T. Ngan, R. Haiges, K. O. Christe, and D. A. Dixon, Energetics and mechanism of the decomposition of trifluoromethanol, J. Phys. Chem. A **112**, 1298 (2008).

[39] N. R. Gulvi, P. J. Maliekal, M. G. Mapari, and P. M. Badani, Theoretical kinetic analysis and molecular dynamic simulations for exploring the dissociation pathways of CF$_3$OH, Comput. Theor. Chem. **1194**, 113056 (2021).

[40] L. G. Huey, P. W. Villalta, E. J. Dunlea, D. R. Hanson, and C. J. Howard, Reactions of CF$_3$O$^-$ with atmospheric trace gases, J. Phys. Chem. **100**, 190 (1996).

[41] S. Park, S. Y. Jeong, T. K. Lee, M. W. Park, H. Y. Lim, J. Sung, J. Cho, S. K. Kwak, S. Y. Hong, and N.-S. Choi, Replacing conventional battery electrolyte additives with dioxolone derivatives for high-energy-density lithium-ion batteries, Nat. Commun. **12**, 838 (2021).

[42] K. O. Christe, J. Hegge, B. Hoge, and R. Haiges, Convenient access to trifluoromethanol, Angew. Chem. Int. Ed. **46**, 6155 (2007).

[43] M. Bonomi *et al.*, Promoting transparency and reproducibility in enhanced molecular simulations, Nat. Methods **16**, 670 (2019).

[44] G. A. Tribello, M. Bonomi, D. Branduardi, C. Camilloni, and G. Bussi, PLUMED 2: New feathers for an old bird, Comput. Phys. Commun. **185**, 604 (2014).

[45] S. Kumar, J. M. Rosenberg, D. Bouzida, R. H. Swendsen, and P. A. Kollman, The weighted histogram analysis method for free-energy calculations on biomolecules. I. The method, J. Comput. Chem. **13**, 1011 (1992).

[46] A. Grossfield, WHAM: The weighted histogram analysis method, http://membrane.urmc.rochester.edu/content/wham (2002).